Solitons and Pattern Formation in Liquid Crystals in a Rotating Magnetic Field

Kalman B. Migler and Robert B. Meyer
The Martin Fisher School of Physics, Brandeis University, Waltham, Massachusetts 02254
(Received 16 October 1990)

We have discovered novel nonlinear dissipative dynamic patterns in nematic liquid crystals under the influence of a continuously rotating magnetic field. We present a state diagram of the soliton structures as a function of field and rotation rate and discuss physical models describing their growth and propagation and transitions.

PACS numbers: 61.30.Gd, 47.20.−k, 61.30.Eb

The physics of pattern formation in systems driven far from equilibrium is currently the subject of intense theoretical and experimental effort. Two prototypical examples are hydrodynamic instabilities[1] and pattern-forming chemical reaction-diffusion systems.[2] Liquid crystals also provide an excellent system to study nonlinear pattern-forming behavior.[3] Stimulated by these works, we reexamine the case of a nematic liquid crystal (NLC) in a continuously rotating magnetic field and find novel nonlinear dynamic structures. We have observed several types of soliton structures. In this Letter we present a state diagram of the patterns and discuss models to describe their formation and growth. In particular, we have discovered that a viscosity reduction mechanism accounts for many of the observed features. The variety of dynamic patterns coupled with the ease of observation and simplicity of experimentation makes this an attractive system to study.

The experiment employs a low-molecular-weight room-temperature NLC blend (E31lv, manufactured by BDH). The NLC is sandwiched between two glass plates of radius R separated by a distance d ($R \gg d$), where the z direction is perpendicular to the glass plates. All measurements on the system were done at room temperature. The liquid crystal is homeotropically aligned; i.e., the director is perpendicular to the glass plates at the plate boundaries. The director $\hat{\mathbf{n}}$ is described by the usual polar angles ($n_z = \cos\theta$, $n_x = \sin\theta\cos\phi$). A homogeneous magnetic field of strength H, parallel to the x-y plane, rotates with angular frequency ω about the z axis. (In the laboratory frame, the sample rotates in a static field.) The sample is placed between crossed polarizers and illuminated with white light.

In this Letter, we will examine patterns in the x-y plane which occur for fields well above $H_c(\omega)$, the Frederiks transition threshold. A previous theoretical search for pattern formation in the small-θ approximation yielded negative results.[4] In the high-field limit, Brochard, Lèger, and Meyer[5] identified the two principle states for a homogeneous (in the x-y plane) sample; synchronous and asynchronous. The synchronous state exists when $\omega\tau < 1$, where $\tau = 2\gamma_1/\chi_a H^2$ (γ_1 and χ_a are respectively the rotational viscosity and the anisotropy of the diamagnetic susceptibility). This state is characterized by a constant-phase lag angle $\alpha = \omega t - \phi$ between $\mathbf{H}$ and $\mathbf{n}_\perp$, the projection of $\hat{\mathbf{n}}$ in the x-y plane. The condition for the asynchronous state is $\omega\tau > 1$ and it is characterized by a continuously increasing phase lag angle.[5] The period of the asynchronous regime is defined by the time for α to increase by π:

$$T_h = \pi\tau/[(\omega\tau)^2 - 1]^{1/2}. \quad (1)$$

Note the basic reason for the use of homeotropic boundary conditions: In a strong field the director in the mid-region rotates about the z axis, while the two thin boundary layers in which the director varies from $\theta = 0$ at the glass plates to $\theta \approx \pi/2$ in the bulk act as pivot or slip surfaces for the director. Therefore, the director can continuously rotate in a homogeneous state without an increase in elastic energy.

Magnetically induced solitary waves (also called walls or kinks) in NLC were first discovered by Helfrich.[6,7] In the synchronous regime, we have discovered the existence of what we call *dynamic solitons* (see Fig. 1). A soliton is the thin region separating two energetically equivalent but topologically distinct domains of the sample which differ in ϕ by an amount π. The director varies smoothly through the soliton. A dynamic soliton must be nucleated either by a dust particle, in which case it moves outward as a growing circular ring, or by the outer sidewall of the sample, in which case it moves inward as a shrinking circular ring.

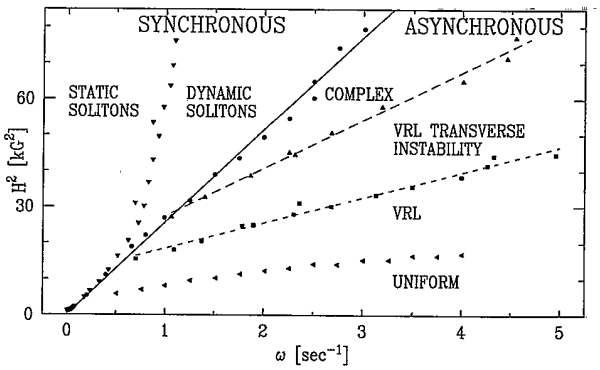

FIG. 1. The experimental state diagram showing the pattern-forming states above the Frederiks transition.

The overdamped sine-Gordon equation models the soliton to a first approximation. In order to simplify the theoretical description while retaining certain results, several approximations are made: We use the approximation $K=K_1=K_3$, where K_1 and K_3 are respectively the splay and bend elastic constants; we do not explicitly consider the effect of fluid backflow on the director; we neglect any variation of α with z; and we assume that the director in a soliton remains in the x-y plane. This last assumption breaks down in the *static soliton* state. The one-dimensional torque equation about the z axis [valid when the radius of a soliton ring is much larger than the magnetic coherence length, $l_c=(K/\chi_a H^2)^{1/2}$] is

$$K\partial_x^2\alpha-\gamma_1\frac{\partial\alpha}{\partial t}+\gamma_1\omega-\tfrac{1}{2}\chi_a H^2\sin 2\alpha=0. \qquad (2)$$

It is well known that a soliton solution of Eq. (2) of the form $\alpha=\alpha(x-vt)$ exists where x is a coordinate normal to the soliton and v is its velocity.[8] A natural velocity scale is given by $v_0=l_c/\sqrt{2}\tau$. In order to test the above theory, we measured the velocity of outward-growing isolated ring solitons as a function of ω for $H=7.09$ kG. In order to insure that the one-dimensional limit is valid, i.e., $r_s\gg l_c$, we worked with solitons of radius $r_s>1$ mm whereas $l_c=3.5$ μm for the above value of H. Using the above value for H, and other measured parameters, we find that $v_0=9.9$ μm s^{-1}. Figure 2 shows the experimental data along with the theoretical curve. While the magnitude of the velocity is well predicted by Eq. (2), the shape of the theoretical and experimental curves differ. In particular, the experiment does not show a divergence of the velocity as $\omega\tau$ approaches 1 as predicted by the sine-Gordon equation. It is likely that incorporation of fluid-backflow effects will produce improved agreement.

A dust particle can nucleate a soliton lattice (train) by locally creating a region of increased viscous drag. Near a dust particle, α is increased from its value of α_0 in the bulk. Elastic forces acting in the plane of the sample will inhibit the growth of α near the dust particle. However, if the increased drag is strong enough, a soliton, i.e., a phase increase of π, will nucleate at the dust particle and propagate outward. This temporarily relaxes the elastic torque at the dust particle. At small radius, a soliton has a line tension which creates a retarding force on its outward growth which falls off as $1/r$. Overcoming this force, the soliton propagates away and another soliton can be nucleated, forming a soliton lattice.

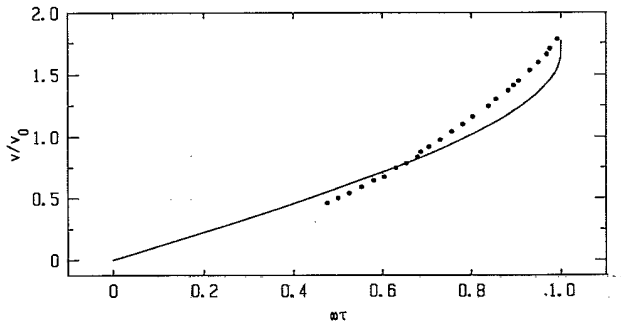

FIG. 2. Theoretical and experimental plot of the velocity of an isolated ring soliton as a function of ω for constant H.

The dynamics of a sample containing numerous soliton sources is governed by soliton interactions. Two regions separated by an odd number of solitons are physically distinct while regions separated by an even number are physically equivalent. Thus when two solitons nucleated from different parts of the sample collide, they mutually annihilate at the point of contact [see Fig. 3(a)].

In Fig. 2, the velocity drops discontinuously to 0 at $\omega\tau=0.48$ indicating a structural transition from a *dynamic soliton* to a *static soliton*. In Fig. 1 the transition line represents the points where a dynamic soliton transforms into a static soliton upon decreasing ω. This transition is observed by removing the analyzer and rotating the polarizer so that the polarization of the incident light is perpendicular to $n_\perp$, as defined in the homogeneous region. In a dynamic soliton, there is a focusing effect which causes the soliton to appear dark relative to the background. But in a static soliton, there is a sharp decrease in the optical contrast between the soliton and the background. This indicates optically that in a static soliton, the director twists out of the x-y plane, so it is similar to solitons described by Brochard and Leger.[7] By twisting out of plane, it reduces elastic energy by replacing splay and bend with twist. Static solitons do not propagate because the $\partial_x^2\alpha$ torque term has no component in the z direction. Additionally, we observe a hysteresis effect when cycling a soliton through this transition point, indicating a bistability of the soliton structures.

In the asynchronous regime, we propose a viscosity reduction mechanism to explain the novel dynamic structures. We classify them according to dimensionality and formation from an initially homogeneous sample. For a given H and ω, the sample is initially placed in a field of strength H at $\omega=0$ so that a uniform Frederiks transition takes place. The rotation is quickly turned on, the system is allowed to evolve, and the pattern type is deduced by visual inspection.

The *viscosity reduction lattice* (VRL) is the simplest of the asynchronous patterns. Starting from an initially homogeneous sample, VRLs are observed to nucleate off of dust particles and off of the outer sidewalls. As the lattices grow into the homogeneous sample, there is a well-defined VRL-homogeneous boundary until the VRLs fill the entire sample. In a dust-particle-nucleated VRL, for example, solitons are formed at the lattice-homogeneous boundary at a rate of $1/T_h$ and propagate inward towards the dust particle until they shrink up and disappear. The location where the outermost soliton is formed each time moves slightly further into the homogeneous region causing a growth in both the radius and

number of wavelengths of the lattice. A wavelength is defined as the distance for α to increase by π in the radial direction. α is a monotonically increasing function of position from the center of a dust-particle-nucleated VRL. This implies that $\alpha_l(t) < \alpha_h(t)$, in sharp contrast to a dynamic soliton lattice in the synchronous regime where $\alpha_l(t) > \alpha_h$. (The subscript l or h refers respectively to the lattice region or the homogeneous region.)

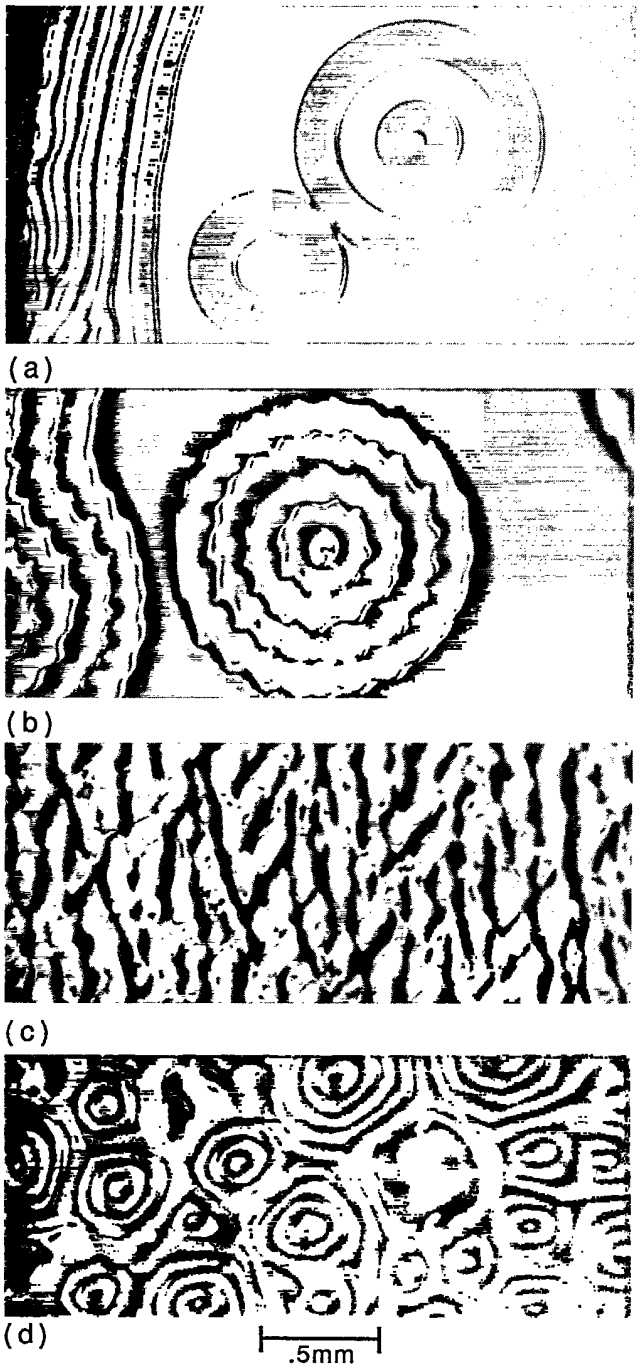

FIG. 3. Photographs of (a) *dynamic solitons* nucleating off of the outer side boundary and off of dust particles, (b) *VRL transverse instability* nucleated from outer side boundary and dust particle as it grows into an initially homogeneous sample, (c) initial development of *complex* state after about 5 s, and (d) long-term structure in *complex* state.

To explain the stability of the VRL relative to the homogeneous state, we invoke a viscosity reduction mechanism. Fluid flow can occur in regions of the sample where $\partial_x \dot{\alpha} \neq 0$. In the appropriate geometry, spatial gradients in fluid flow in turn create a positive feedback torque on the director which has the net effect of reducing the effective viscosity for director rotation.[9] In this case, the lower viscosity in the VRL allows it to follow the rotating field more closely; i.e., the time-averaged value of $\dot{\alpha}_l < \dot{\alpha}_h$, which implies $\alpha_l < \alpha_h$ throughout the VRL. The magnitude of this effect is shown in Fig. 4 where the period of α in the homogeneous region is compared with the longer period in the lattice for an outer-sidewall-nucleated VRL; simultaneously, the wavelength is measured. As H is decreased, the period difference goes to 0 at the same point that the wavelength diverges, signaling the onset of the uniform state.

The viscosity reduction mechanism is necessary to explain the growth of the lattice into the homogeneous region. The condition for the growth of the lattice is that the soliton formation rate T_h^{-1} is greater than the current of solitons through a given point in the lattice; $v/\lambda < T_h^{-1}$, where v is the velocity of the solitons. In the long-wavelength limit, where elastic forces in the lattice are negligible, the above inequality follows directly from $\gamma_{1l} < \gamma_{1h}$. Our numerical simulations which include the effects of backflow and elasticity confirm the viscosity reduction mechanism outlined above.

Nucleation of a VRL by a dust particle, which locally increases viscous drag, sounds like a contradiction. However, an initially homogeneous sample is metastable (rather than unstable) with respect to a VRL. The role of the dust particle is to create a local disturbance which initiates the viscosity-reducing backflow and nucleates a VRL. It is sometimes observed that as a dust-particle-nucleated VRL grows, the center of it slowly drifts away from the dust particle. Clearly, the dust particle is only

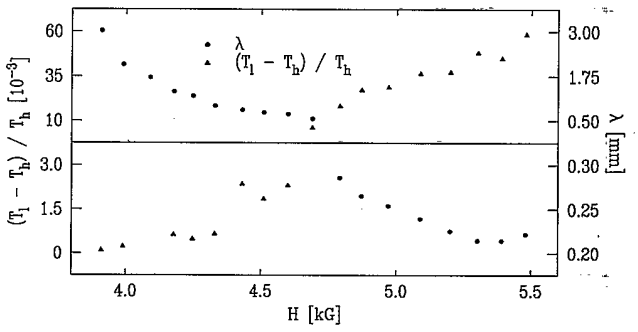

FIG. 4. Plot of the wavelength of the VRL and the difference between the period of this lattice and that of the homogeneous region for $\omega = 2.5\ s^{-1}$. Note the jump in scale.

important for nucleation of the VRL, not the subsequent dynamics.

The section of the state diagram labeled *VRL transverse instability* (VRL-TI) marks a bifurcation in the state diagram. The VRL-TI is similar to the above VRL in most manners except that there is also a periodic distortion with wave vector parallel to the lattice-homogeneous boundary. In Fig. 3(b), this transverse distortion is the ripples on the concentric rings around the dust particle in the center of the picture. The most likely explanation for this effect is again the backflow. The previously discussed VRL (no photograph) is qualitatively similar in appearance to Fig. 3(b) except there are no ripples on the rings.

Insight to the *complex* pattern state can be gained by observing the nucleation of lattices by dust particles in the VRL-TI state. In a given sample, there is a distribution of dust particle sizes and generally only the bigger ones nucleate lattices. However, as the conditions are moved closer to the complex pattern state, progressively smaller-sized dust particles are capable of nucleating lattices. Finally, at the transition between the VRL-TI and complex pattern states, the size of a dust particle needed to nucleate a lattice goes to zero. Wavelike fluctuations appear spontaneously and grow throughout the sample. Thus in the complex pattern state, an initially homogeneous sample is unstable to fluctuations. In the long-term dynamics, there is a competition between localized lattice segments which evolve into an array of multiple-wavelength ringlike lattices [see Figs. 3(c) and 3(d)].

In conclusion, we have explored the pattern-forming aspects of a nematic liquid crystal in a rotating magnetic field with emphasis on its soliton structures. In the synchronous regime, dynamic solitons and static solitons have been observed. In the asynchronous regime, the coupling of the director motion with fluid flow creates novel dynamic patterns, and a variety of structural transitions.

This research was supported by the National Science Foundation through Grant No. DMR-8803582, and by the Martin Fisher School of Physics, Brandeis University.

[1] *Propagation in Systems far from Equilibrium,* edited by J. Wesfreid, H. Brand, P. Monneville, G. Albinet, and N. Boccara (Springer-Verlag, Berline, 1988).

[2] *Oscillations and Traveling Waves in Chemical Systems,* edited by R. J. Field and M. Burger (Wiley, New York, 1985).

[3] "Solitons in Liquid Crystals," edited by L. Lam and J. Prost (Springer-Verlag, Berlin, to be published).

[4] F. Sagués, Phys. Rev. A **38**, 5360 (1988).

[5] F. Brochard, L. Lèger, and R. B. Meyer, J. Phys. (Paris), Colloq. **36**, C1-209 (1975).

[6] W. Helfrich, Phys. Rev. Lett. **21**, 1518 (1968).

[7] F. Brochard, J. Phys. (Paris) **33**, 607 (1972); L. Leger, Solid State Commun. **11**, 1499 (1972); **24**, 33 (1973).

[8] M. Buttiker and R. Landauer, Phys. Rev. A **23**, 1397 (1981); S. E. Burkov, V. L. Pokrovsky, and G. V. Uimin, Solid State Commun. **40**, 363 (1981).

[9] E. Guyon, R. Meyer, and J. Salan, Mol. Cryst. Liq. Cryst. **54**, 261 (1979).